PERGAMON

International Journal of Heat and Mass Transfer 41 (1998) 3559–3573

International Journal of HEAT and MASS TRANSFER

Heat transfer enhancement in three-dimensional corrugated channel flow

David R. Sawyers[a], Mihir Sen[b,*], Hsueh-Chia Chang[c]

[a] *Department of Mechanical and Materials Engineering, Wilkes University, Wilkes-Barre, PA 18766, U.S.A.*
[b] *Department of Aerospace and Mechanical Engineering,* [c] *Department of Chemical Engineering, University of Notre Dame, Notre Dame, IN 46556, U.S.A.*

Received 7 August 1997; in final form 27 December 1997

Abstract

The effect of three-dimensional hydrodynamics on the enhancement of steady, laminar heat transfer in corrugated channels is studied using a combination of analytical and numerical techniques. Reynolds numbers are considered in the range of $0 < Re < 250$ to avoid unsteady flow. Two-dimensional sinusoidal corrugations with flow perpendicular to the corrugations is taken as the base. The heat transfer is higher than for flat plates due to the presence of recirculation zones; there is increased advection near each stagnation point which, when combined with the asymmetry of the flow in the downstream direction, leads to a larger area-averaged heat transfer coefficient. In the three-dimensional case the corrugations are sinusoidal in two orthogonal directions. A small mean flow in the transverse direction leads to an increase in the heat transfer by allowing particles to cross between the recirculation zones and the main flow. As the transverse flow becomes stronger, the recirculation is destroyed and there is a corresponding decrease in heat transfer.

Nomenclature

A corrugated surface area of wall
c specific heat of fluid
$\hat{d}$ average separation between plates
g determinant of covariant metric tensor
g^{ij} contravariant metric tensor
h heat transfer coefficient
k thermal conductivity
n normal to wall
Nu local Nusselt number
$\langle Nu \rangle$ area-averaged Nusselt number
$\langle Nu_0 \rangle$ area-averaged Nusselt number for zero Peclet number
p pressure
Pe Peclet number, $Pe = U\hat{d}\rho c/k$
Re Reynolds number, $Re = U\hat{d}/v$
$s(x, z)$ shape of channel walls
t time
T temperature
T_H^*, T_C^* temperature of hot and cold walls, respectively
u, v, w cartesian velocity components
u^i covariant velocity component
x, y, z cartesian coordinates
$\mathbf{X}$ fluid particle position
U mean flow velocity in channel
$\mathbf{V}$ velocity vector
V_w magnitude of near-wall velocity.

Greek symbols

α angle of flow to x-axis
β_i amplitudes of corrugations in i-direction ($i = x, z$)
λ_i wavelengths of corrugations in i-direction ($i = x, z$)
v kinematic viscosity of fluid
ρ density of fluid
χ, η, ζ boundary-fitted coordinates.

Subscripts

0, 1, ... order of perturbation solution
,i partial differentiation with respect to i-direction ($i = x, y, z$)
sym artificial, symmetric velocity field.

* Corresponding author.

0017–9310/98 $19.00
PII: S0017–9310(98)00029–5

Superscripts
* dimensional quantity
˜ rescaled nondimensional quantity.

1. Introduction

Plate heat exchangers are common in the process industry. Heat transfer in these devices can be increased by introducing some form of mixing into the flow which reduces nonuniformities in the temperature of the fluid, thereby steepening the temperature gradient near the boundaries and increasing the heat transfer between the fluid and the channel walls. Because turbulent flows typically exhibit good mixing, it is usual to operate heat exchangers at high flow rates and within the turbulent regime, or to put grooves at the walls or inserts in the flow which promote turbulent flow. However, compared to laminar flow turbulence requires a significant increase in the energy needed to drive the system, especially for very viscous fluids or for small compact heat exchangers. In such systems, it is advantageous to use geometries which have good laminar mixing characteristics.

Laminar mixing can be induced by different nonplanar wall geometries in which the flow separates at a wall [1, 2]. This has been used to enhance heat transfer in two-dimensional flows. Various wall geometries have been tried : sawtooth [3] and stepped [4] geometries have been proposed ; sinusoidal shapes, either sinuous [5–9] or varicose [1, 10], have also been studied. Smooth shapes are easier to handle with analytical or numerical techniques. Enhancement of both heat and mass transfer as compared to planar walls has been experimentally verified.

It is possible to enhance heat transfer further by moving away from two-dimensional, steady flow. It is known that the bounding streamlines of recirculation zones can be broken up by periodic, small perturbations resulting in increased heat transfer. In the language of dynamical systems theory, a homoclinic or heteroclinic orbit breaks up due to the entanglement of stable and unstable manifolds and produces a stochastic layer. Chaotic particle paths may appear in two-dimensional, non-autonomous or three-dimensional, autonomous systems. In the case of fluid motion, the velocity vector provides the vector field for particle paths. Ghosh et al. [11] applied a time-periodic oscillation to a journal-bearing flow to show this effect. Acharya et al. [12] achieved similar results in helical pipes by spatial periodicity in the downstream direction. In these examples, chaotic particle paths have been shown to increase mixing and hence the heat transfer rate [13]. It may thus be possible to apply this idea to plate heat exchangers and increase heat transfer by changing from steady, two-dimensional to steady, three-dimensional flow. There are many different channel geometries which can give rise to three-dimensionality in the flow. The simplest is two-dimensional corrugations in which the flow comes at an angle to the corrugations. Or we can have three-dimensional corrugations in one of several different patterns. Most of the work done on three-dimensional flow in channels has been on turbulent flows with herringbone patterns [14–16]. Laminar flow in this geometry has been experimentally studied by Focke et al. [17]. Focke and Knibbe [18] have shown by flow visualization that very complicated pathlines exist, indicating good mixing and the possibility of improved heat transfer.

We are interested in understanding the mechanism and extent of heat transfer enhancement by three-dimensionality in steady, laminar channel flows. The base flow to which heat transfer will be compared is a channel with two-dimensional, sinusoidal, varicose corrugations, schematically shown in Fig. 1(a), in which the flow is perpendicular to the corrugations. Then we add corrugations in the normal direction to produce the three-dimensional geometry shown in Fig. 1(b) (which we will refer to hereafter as the 'eggcarton' configuration). These two channel geometries will enable us to carry out per-

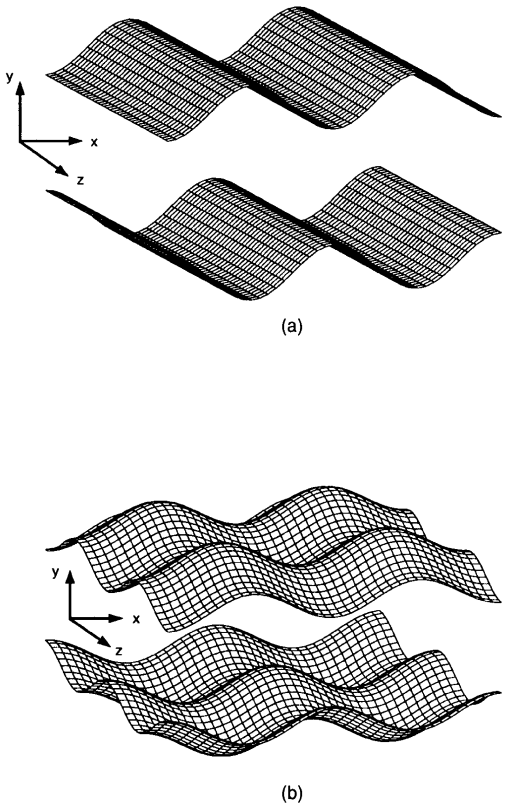

Fig. 1. Channels with (a) two-dimensional and (b) eggcarton corrugations.

turbation analyses, for suitable small parameters, of the two- and three-dimensional hydrodynamics. Numerical integration of the velocity fields gives us pathlines which will provide a qualitative picture of the mixing. In addition, finite-volume numerical solutions will be used to extend the range of the hydrodynamical results outside the validity of the perturbation solution, as well as to determine the temperature field and heat transfer rates. To avoid unsteady flow we will confine all our results to a maximum Reynolds number of 250.

2. Problem definition

We consider the steady, laminar flow between corrugated plates of an incompressible Newtonian fluid with constant properties. The coordinate system (x, y, z) is shown in Fig. 1. The flow is produced by an imposed pressure gradient in the x–z plane at an angle α with respect to the x-axis. The walls are kept at different temperatures so that the heat transfer is primarily from one to the other. Given a fixed geometry, the pressure drop and volume flow rate in the channel are related, so that one determines the other. Here we will prescribe the flow rate through specification of the Reynolds number; the velocity and pressure fields will be unknown.

The governing equations are nondimensionalized using the average separation between the channel walls as the characteristic length $\hat{d}$, the mean inlet velocity as the characteristic speed U, and ρU^2 as the characteristic pressure, where ρ is the density. The nondimensional mean flow velocity is thus unity with components $\cos\alpha$ and $\sin\alpha$ in the x- and z-directions, respectively. The temperature is nondimensionalized as

$$T = \frac{T^* - T_C^*}{T_H^* - T_C^*} \tag{1}$$

where T_H^* and T_C^* are the temperatures of the upper and lower walls, respectively. All variables from now on are nondimensional.

The mass, momentum and energy balance equations are

$$\nabla \cdot \mathbf{V} = 0 \tag{2}$$

$$(\mathbf{V} \cdot \nabla)\mathbf{V} = \frac{1}{Re}\nabla^2 \mathbf{V} - \nabla p \tag{3}$$

$$(\mathbf{V} \cdot \nabla)T = \frac{1}{Pe}\nabla^2 T \tag{4}$$

where viscous dissipation has been neglected. $\mathbf{V} = (u, v, w)$ and p are the velocity and pressure, respectively. The Reynolds and Peclet numbers are given by $Re = U\hat{d}/\nu$ and $Pe = U\hat{d}\rho c/k$, respectively. The Peclet number is a measure of the importance of advective to conductive heat transfer.

The walls of the channel are at $y = \pm s$, where

$$s(x, z) = \frac{1}{2} + \beta_x \cos\left(\frac{2\pi x}{\lambda_x}\right) + \beta_z \cos\left(\frac{2\pi z}{\lambda_z}\right) \tag{5}$$

where β_x and λ_x are the dimensionless amplitude and wavelength of the corrugations in the x-direction, and β_z and λ_z are those in the z-direction. $\beta_z = 0$ is a special case of two-dimensional corrugations; the flow, however, is two-dimensional only if $\alpha = 0$ also.

For simplicity, we will limit ourselves to fully-developed velocity and temperature fields that are far from the localized effects of inlet and outlet sections. This requires periodicity in the flow variables over λ_x and λ_z in the x- and z-directions, respectively. Thus, only one wavelength in these two directions need be considered. The boundary conditions are the following:

- *Velocity*: $\mathbf{V}$ is zero at the upper and lower walls due to no-slip, and is periodic in the x- and z-directions
- *Temperature*: $T = 0$ at $y = -s$, and $T = 1$ at $y = s$; T is also periodic in the x- and z-directions.
- *Pressure*: The pressure gradient is periodic in the x- and z-directions. The condition for pressure in the y-direction is somewhat more complicated. For the perturbation solution $\partial p/\partial y$ does not appear in the leading or first order equations, so a boundary condition is not necessary. In the numerical solution, a condition for pressure at the walls is obtained from the momentum equation.

Heat transfer in the channel will be quantified in terms of the Nusselt number at a wall defined as

$$Nu \equiv \frac{hd}{k} = \left|\frac{\partial T}{\partial n}\right| \tag{6}$$

where h is the heat transfer coefficient, k is the thermal conductivity of the fluid, and $\partial T/\partial n$ is the temperature gradient normal to a wall. The global heat transfer is represented by the area-averaged Nusselt number

$$\langle Nu \rangle = \frac{1}{A}\int\int_A \left.\frac{\partial T}{\partial n}\right|_{y=s} \mathrm{d}z\,\mathrm{d}x \tag{7}$$

where A is the surface area of either of the corrugated channel walls. In order to assess the effect of advection, we will often determine the heat transfer rate as a function of Peclet number. Since $Pe = 0$ corresponds to pure conduction, the Nusselt number presented will, in these cases, be normalized with respect to its value at $Pe = 0$, written as $\langle Nu_0 \rangle$.

3. Perturbation solution

Pathlines $\mathbf{X}(\mathbf{X}_0, t)$ can be obtained from the velocity field as solutions of the dynamical system

$$\frac{\mathrm{d}\mathbf{X}}{\mathrm{d}t} = \mathbf{V} \tag{8}$$

where $\mathbf{X} = \mathbf{X}_0$ at time $t = 0$. From a Lagrangian point of view, analysis of particle paths is a key step to understanding mixing. These can be generated much more accurately from continuous, analytical velocity fields than from numerical solutions at discrete points, especially in the presence of chaotic advection where there is extreme sensitivity to an initial position $\mathbf{X}_0$.

To obtain a perturbation solution of the two-dimensional hydrodynamics we will assume that the wavelength is much longer than the average separation distance between the walls, i.e. $\lambda_x \gg 1$, to enable an expansion in terms of the small parameter λ_x^{-1}. For the three-dimensional problem, we will also assume that $\lambda_x \ll \lambda_z$, i.e. the wavelength of corrugations in the z-direction is much larger than that in the x-direction, and that α is small. These assumptions will decouple the solution of the w velocity from u and v at lower orders of λ_x^{-1}.

The relative magnitudes of the terms in the governing equations can be written in terms of λ_x^{-1}. Since variations in the x-direction are smaller than those in the y-direction, x can be rescaled as $x = \lambda_x \tilde{x}$. The secondary flow is also small, so that we can rescale the v velocity component as $v = \lambda_x^{-1}\tilde{v}$. For the three-dimensional problem the z-coordinate can be redefined as $z = \lambda_x^2 \tilde{z}$. The pressure is rescaled as $p = \lambda_x \tilde{p}$ in order to obtain nonzero leading order velocities. The flow angle is changed to $\alpha = \lambda_x^{-1}\tilde{\alpha}$. The rescaled variables $\tilde{x}$, $\tilde{v}$, $\tilde{z}$, $\tilde{p}$ and $\tilde{\alpha}$ are now of unit order.

In terms of the rescaled variables the governing differential equations (2) and (3) become

$$\frac{\partial u}{\partial \tilde{x}} + \frac{\partial \tilde{v}}{\partial y} + \lambda_x^{-1}\frac{\partial w}{\partial \tilde{z}} = 0 \tag{9}$$

$$\lambda_x^{-1}u\frac{\partial u}{\partial \tilde{x}} + \lambda_x^{-1}\tilde{v}\frac{\partial u}{\partial y} + \lambda_x^{-2}w\frac{\partial u}{\partial \tilde{z}} = \frac{1}{Re}\left[\lambda_x^{-2}\frac{\partial^2 u}{\partial \tilde{x}^2} + \frac{\partial^2 u}{\partial y^2} + \lambda_x^{-4}\frac{\partial^2 u}{\partial \tilde{z}^2}\right] - \frac{\partial \tilde{p}}{\partial \tilde{x}} \tag{10}$$

$$\lambda_x^{-3}u\frac{\partial \tilde{v}}{\partial \tilde{x}} - \lambda_x^{-3}\tilde{v}\frac{\partial \tilde{v}}{\partial y} + \lambda_x^{-4}w\frac{\partial \tilde{v}}{\partial \tilde{z}} = \frac{1}{Re}\left[\lambda_x^{-4}\frac{\partial^2 \tilde{v}}{\partial \tilde{x}^2} + \lambda_x^{-2}\frac{\partial^2 \tilde{v}}{\partial y^2} + \lambda_x^{-6}\frac{\partial^2 \tilde{v}}{\partial \tilde{z}^2}\right] - \frac{\partial \tilde{p}}{\partial y}. \tag{11}$$

$$\lambda_x^{-1}u\frac{\partial w}{\partial \tilde{x}} + \lambda_x^{-1}\tilde{v}\frac{\partial w}{\partial y} + \lambda_x^{-2}w\frac{\partial w}{\partial \tilde{z}} = \frac{1}{Re}\left[\lambda_x^{-2}\frac{\partial^2 w}{\partial \tilde{x}^2} + \frac{\partial^2 w}{\partial y^2} + \lambda_x^{-4}\frac{\partial^2 w}{\partial \tilde{z}^2}\right] - \lambda_x^{-1}\frac{\partial \tilde{p}}{\partial \tilde{z}}. \tag{12}$$

A perturbation solution is obtained by expanding the unknowns in the form

$$\phi = \phi_0 + \lambda_x^{-1}\phi_1 + \lambda_x^{-2}\phi_2 + \cdots \tag{13}$$

where ϕ is u, $\tilde{v}$, w, and $\tilde{p}$.

The mean velocities in the x- and z-directions can be expanded as

$$\cos \lambda_x^{-1}\tilde{\alpha} = 1 - \lambda_x^{-2}\frac{\tilde{\alpha}^2}{2!} + \cdots \tag{14}$$

$$\sin \lambda_x^{-1}\tilde{\alpha} = \lambda_x^{-1}\tilde{\alpha} - \lambda_x^{-3}\frac{\tilde{\alpha}^3}{3!} + \cdots \tag{15}$$

respectively.

The $O(1)$ problem gives the velocity field

$$u_0 = \frac{Re}{2}\frac{\partial \tilde{p}_0}{\partial \tilde{x}}(y^2 - s^2) \tag{16}$$

$$\tilde{v}_0 = -\frac{Re}{2}\left[\frac{\partial^2 \tilde{p}_0}{\partial \tilde{x}^2}\left(\frac{y^3}{3} - s^2 y + \frac{2}{3}s^3\right) - 2ss_{\tilde{x}}\frac{\partial \tilde{p}_0}{\partial \tilde{x}}(y - s)\right] \tag{17}$$

$$w_0 = 0 \tag{18}$$

where the subscript on s denotes differentiation. When this solution is required to satisfy $\tilde{v}_0 = 0$ at $y = -s$, we obtain an equation that can be integrated to give

$$\frac{\partial \tilde{p}_0}{\partial \tilde{x}} = -\frac{3}{2Re\, s^3}. \tag{19}$$

The constant of integration is chosen to satisfy equation (14) to leading order.

The same procedure applied to $O(\lambda_x^{-1})$ terms gives the first-order velocity components

$$u_1 = -\frac{Re}{1120s^7}[21s_{\tilde{x}}y^6 - 105s_{\tilde{x}}y^4s^2 + 99s_{\tilde{x}}s^4y^2 + 840s^4y^2 - 15s_{\tilde{x}}s^6 - 840s^6] \tag{20}$$

$$\tilde{v}_1 = \frac{Re}{1120s^8}3y[ss_{\tilde{x}\tilde{x}}y^6 - 7s_{\tilde{x}}y^4s^3 + 35s_{\tilde{x}}^2y^4s^2 + 11s_{\tilde{x}\tilde{x}}s^5y^2 - 33s_{\tilde{x}}^2s^4y^2 - 280s_{\tilde{x}}s^4y^2 - 5s_{\tilde{x}\tilde{x}}s^7 + 5s_{\tilde{x}}^2s^6 + 280s_{\tilde{x}}s^6 - 7s_{\tilde{x}}^2y^6] \tag{21}$$

$$w_1 = -\frac{3\tilde{\alpha}}{4s^3}(y^2 - s^2) \tag{22}$$

with the pressure gradients

$$\frac{\partial \tilde{p}_1}{\partial \tilde{x}} = -\frac{3}{70s^3}[-35s_{\tilde{x}\tilde{x}}s - 17s_{\tilde{x}}^3 + 174s_{\tilde{x}}^2 + 6s_{\tilde{x}}ss_{\tilde{x}\tilde{x}}] \tag{23}$$

$$\frac{\partial \tilde{p}_0}{\partial \tilde{z}} = -\frac{3\tilde{\alpha}}{2Re\, s^3}. \tag{24}$$

Two terms of the perturbation expansion are sufficient to capture the qualitative nature of the flow field including the phenomena of separation and recirculation. Convergence of the expansion depends on the values of Re and the corrugation geometry; for the solutions shown here the second term of the expansion is numerically much smaller than the first. The perturbation solutions

are also validated by comparison to the analytical results of Chow and Soda [1] who used a different perturbation procedure. Details are in [19] where the velocity profiles at different sections are shown.

4. Numerical solution

The perturbation solution gives the hydrodynamics of the flow for large wavelength to separation ratio. In order to solve the energy equation as well as to obtain the hydrodynamics outside the range of validity of the perturbation solution, a finite-volume formulation is used. The governing equations are expressed in terms of a nonorthogonal coordinate system

$$\chi = x \tag{25}$$

$$\eta = \frac{y+s}{2s} \tag{26}$$

$$\zeta = z \tag{27}$$

in which $\eta = 0$ and $\eta = 1$ correspond to the channel walls.

Following Eringen [20] we can rewrite equations (2)–(4) in generalized curvilinear coordinates as

$$(g^{1/2}u^i)_{,i} = 0 \tag{28}$$

$$\left(g^{1/2}u^iu^j - \frac{g^{1/2}}{Re}g^{mj}u^i_{,m} - \frac{g^{1/2}}{Re}g^{mj}\begin{Bmatrix} i \\ ml \end{Bmatrix}u^l\right)_{,j} = -g^{1/2}g^{ki}p_{,k} - g^{1/2}\begin{Bmatrix} i \\ jl \end{Bmatrix}u^iu^j \tag{29}$$

$$\left(g^{1/2}u^jT - \frac{g^{1/2}}{Pe}g^{mj}T_{,m}\right)_{,j} = 0 \tag{30}$$

where u^i are the contravariant components of the velocity vector, g^{mj} is the contravariant metric tensor, g is the determinant of the covariant metric tensor, and $\{\}$ is the Christoffel symbol of the second kind. The subscript $,i$ denotes partical differentiation with respect to the ith direction.

These equations are discretized using the power-law scheme of Patankar [21]. The resulting equations are solved using the modified PISO-SIMPLER algorithm of Sharatchandra and Rhode [22]. The key features of this algorithm are: (a) an explicit equation for pressure is obtained from the continuity equation, similar to the SIMPLE-based schemes, and (b) the problem of pressure checkerboarding endemic to non-staggered grids is avoided by application of the momentum equation to obtain a particular interpolation scheme.

The numerical code was validated by comparison to standard results for entrance flow in flat-plate channels and in a square duct, and to the corrugated channel results of Sobey [2]. Convergence with respect to mesh size was also confirmed. A mesh of 31×31 was chosen for the two- and $31 \times 31 \times 31$ for the three-dimensional calculations.

Before proceeding to a discussion of results, it is appropriate to summarize and compare the regions of validity of the analytical and numerical solution procedures. Figure 2 shows a comparison of the size of the unmixed region of the flow, defined as:

$$d = \int_{-\lambda_x/2}^{\lambda_x/2} d'(x)\,\mathrm{d}x \tag{31}$$

where $d'(x)$ is the distance from the upper channel wall to the edge of the recirculation region. The perturbation approach used to obtain analytical solutions presupposes that corrugation wavelengths are much larger than the channel width. The higher order terms which have been neglected depend strongly on Reynolds number, so that as the size of the recirculation region grows, the analytical solutions becomes less accurate. In contrast, the numerical approach provides accurate solutions for small wavelength channels, but has difficulty in resolving small recirculation regions. In the following discussion, numerical results will be reported only for cases where the secondary flow is well-developed. Also, the analytical solutions will be used primarily to understand the qualitative nature of the flow.

5. Two-dimensional corrugations

For this case, $\beta_z = \alpha = 0$ as shown in Fig. 1(a). The corrugations are independent of the z-coordinate and the flow is only in the x-direction.

5.1. Pathlines

Particle paths for a long wavelength channel can be obtained by integrating equation (8) where the vector field $\mathbf{V}$ is given by equations (16)–(22). A fifth-order Runga–Kutta scheme is used to perform the integration. The resulting pathlines are shown in Fig. 3 in the dimensionless coordinate system. The recirculation region near the wall can clearly be seen. There is a bounding streamline which separates the recirculation region from the main channel flow which the fluid does not cross. There is no advection of heat across this streamline, only conduction.

5.2. Pressure drop

Figure 4 shows the effect of Reynolds number on pressure drop for flat and corrugated channel walls. The addition of corrugations has a significant effect at very low Reynolds numbers, increasing the pressure gradient by about 25% for $Re = 25$. However, as Re increases the pressure drop in a corrugated channel becomes indis-

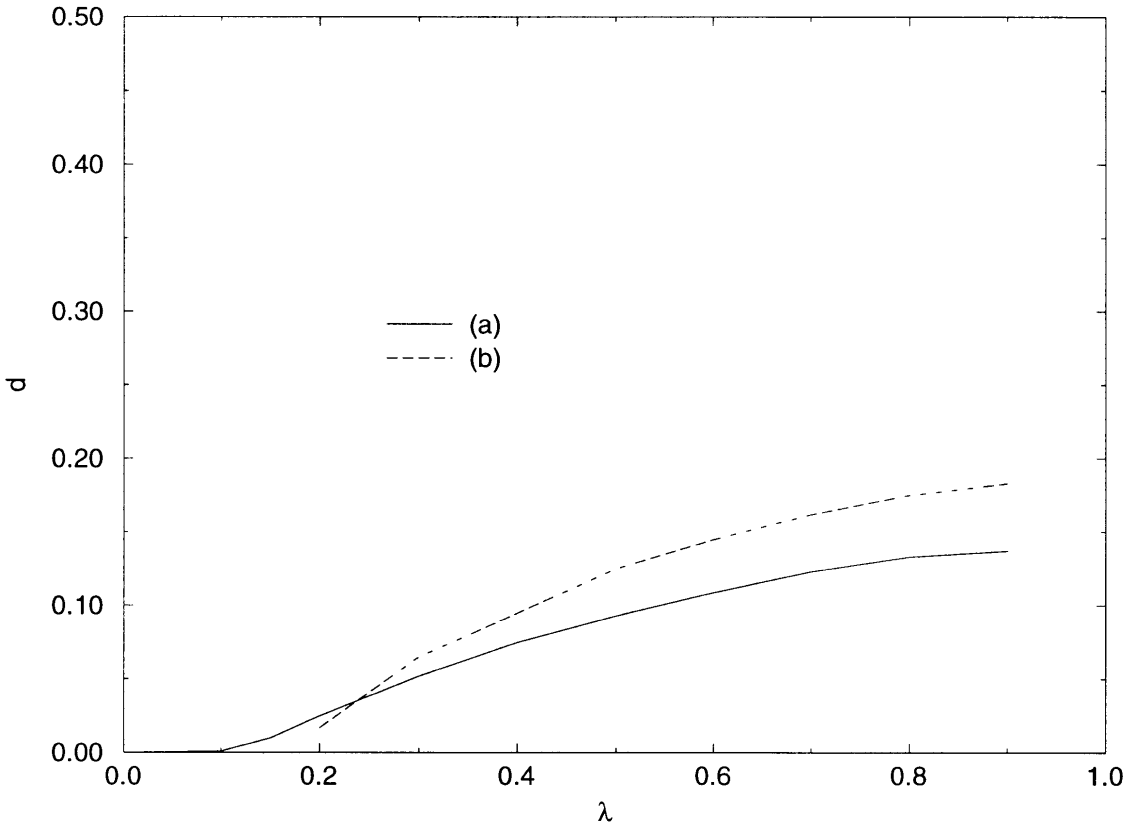

Fig. 2. Comparison of recirculation region size for (a) analytical and (b) numerical solutions with $Re = 100$, $\beta = 0.2$, and $\gamma = 0$.

tinguishable from that for flow between flat plates with the same average separation distance and mass flow rate. Because it becomes very small, it is difficult to make precise comparisons of the pressure drop from the numerical algorithm.

5.3. Heat transfer

Figure 5 shows the distribution of local Nusselt number along the upper wall for fixed Reynolds number and channel geometry. For a very small Peclet number, curve (a), the effect of advection is negligible. At $x = -\lambda_x/2$, $x = 0$ and $x = \lambda_x/2$ the normal to the wall lies in the y-direction, so the Nusselt number at these locations is simply

$$\left|\frac{\partial T}{\partial n}\right| = \frac{1}{2s}. \tag{32}$$

In between these points the curve is distorted purely due to the effects of wall corrugations on conduction heat transfer. As Peclet number increases, the influence of the hydrodynamics of separated flow become apparent. For high Pe there is a decrease in temperature gradient to the left of the channel center where hot fluid is pushed away from the hot wall, and an increase to the right where cold fluid is pushed toward the hot wall.

Integrating the local Nusselt number over one wavelength in the x-direction gives the area-averaged Nusselt number. For the curves shown in Fig. 5, (a) $\langle Nu \rangle = 0.749$, (b) $\langle Nu \rangle = 0.889$, (c) $\langle Nu \rangle = 0.993$, and (d) $\langle Nu \rangle = 1.102$, respectively. The physical reasons for this increase with Pe can be explained by comparing the local Nusselt number with the magnitude of the velocity near the upper wall. The latter is represented by the nearest grid point for which a numerical value, V_w, is available; for convenience, this velocity has been normalized by its value at $x = 0$. Figure 6 shows curve (d) of Fig. 5 along with V_w. It can be seen that the velocity is asymmetric about $x = 0$ and gives more weight to the right stagnation point which produces a local enhancement, than to the left which causes a local inhibition. The result is a net increase in the area-averaged heat transfer which grows as the advection becomes more important.

To confirm that this asymmetry is in fact responsible for heat transfer enhancement, we can compare it with an artificially-produced symmetric flow. Consider the

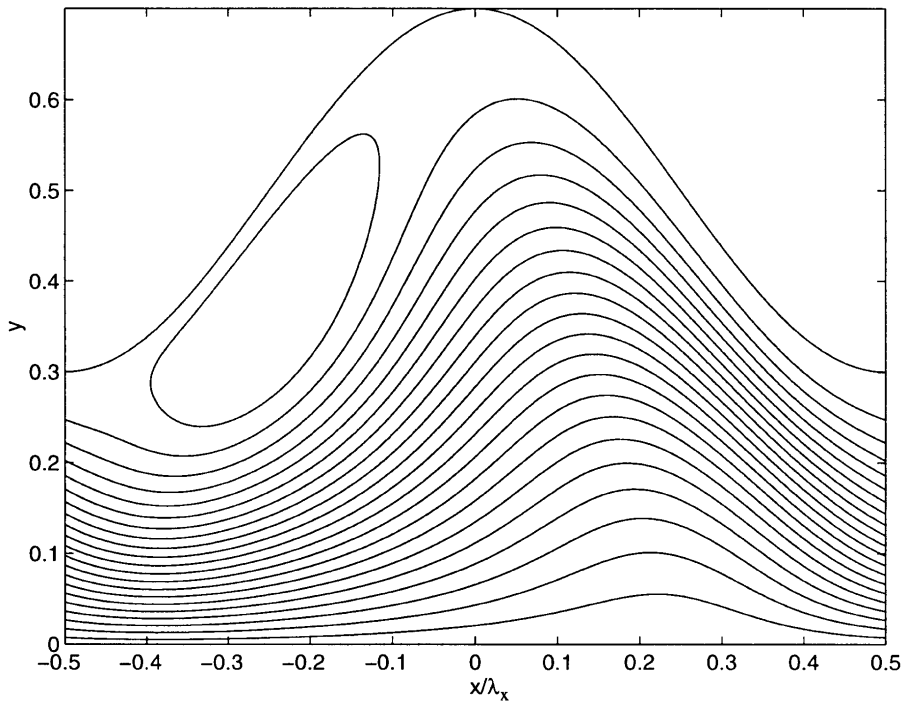

Fig. 3. Two-dimensional corrugations: pathlines from perturbation solution; $Re = 350$, $\beta_x = 0.2$, $\lambda_x = 10$. Main flow from left to right.

numerically-obtained flow pattern shown in Fig. 7. We can produce an artificial flow field u_{sym}, v_{sym} from

$$u_{sym}(x,y) = \tfrac{1}{2}[u(x,y)+u(-x,y)] \quad (33)$$

$$v_{sym}(x,y) = \tfrac{1}{2}[v(x,y)-v(-x,y)] \quad (34)$$

where u and v are the correct numerical results. Figure 8 shows that the enhancement is much greater in the correct asymmetric flow than in the artificial symmetric one, especially as advection becomes more important. The mechanism for heat transfer enhancement in the corrugated channel is therefore a combination of advection near the stagnation points and the asymmetry of the recirculating flow.

6. Eggcarton corrugations

Here we have $\beta_z \neq 0$ as shown in Fig. 1(b). If $\alpha = 0$ the flow is mainly in the x-direction; the three-dimensional corrugations do introduce some three-dimensionality to the flow though there is no mean flow in the z-direction. As α increases the flow acquires a greater mean component in the z-direction.

6.1. Pathlines

Figure 9 shows the paths of particles in an eggcarton-type channel with $\beta_x+\beta_z$ the same as in Fig. 3. The pathlines are significantly different than that in the two-dimensional corrugations, even tough the values of β_z and α are small. The three-dimensionality causes the boundary of the recirculating region to be broken, allowing exchange of fluid between it and the mid-channel flow. The pathline shown by the broken line does several loops within the recirculation region before leaving it. The flow-visualization observations of Focke and Knibbe [18] have shown similar characteristics in which fluid is sucked into a vortex located within a furrow and is eventually pumped out again.

Lyapunov exponents can be used to measure the rate at which an infinitesimal fluid volume is stretched. There is a Lyapunov exponent associated with each dimension of the flow, and for a conservative, incompressible system the sum of these exponents must be zero. For a non-chaotic system, in which stretching occurs at a linear rate, all exponents must be zero. For a system which exhibits chaotic particle paths, the largest Lyapunov exponent is positive, denoting exponential separation of neighboring particles. Note that the Lyapunov exponents are dependent on initial location of the tracer particle. Using the algorithm of Wolf et al. [23] the Lyapunov exponents associated with a certain location within the domain can be found by tracing the path of a single particle with initial conditions at that location. With the velocity field of equations (16)–(22) and a particle initially at $(x,y,z) = (0.0, 0.25, 0.0)$, we find a value of 3.8 ± 0.25 for

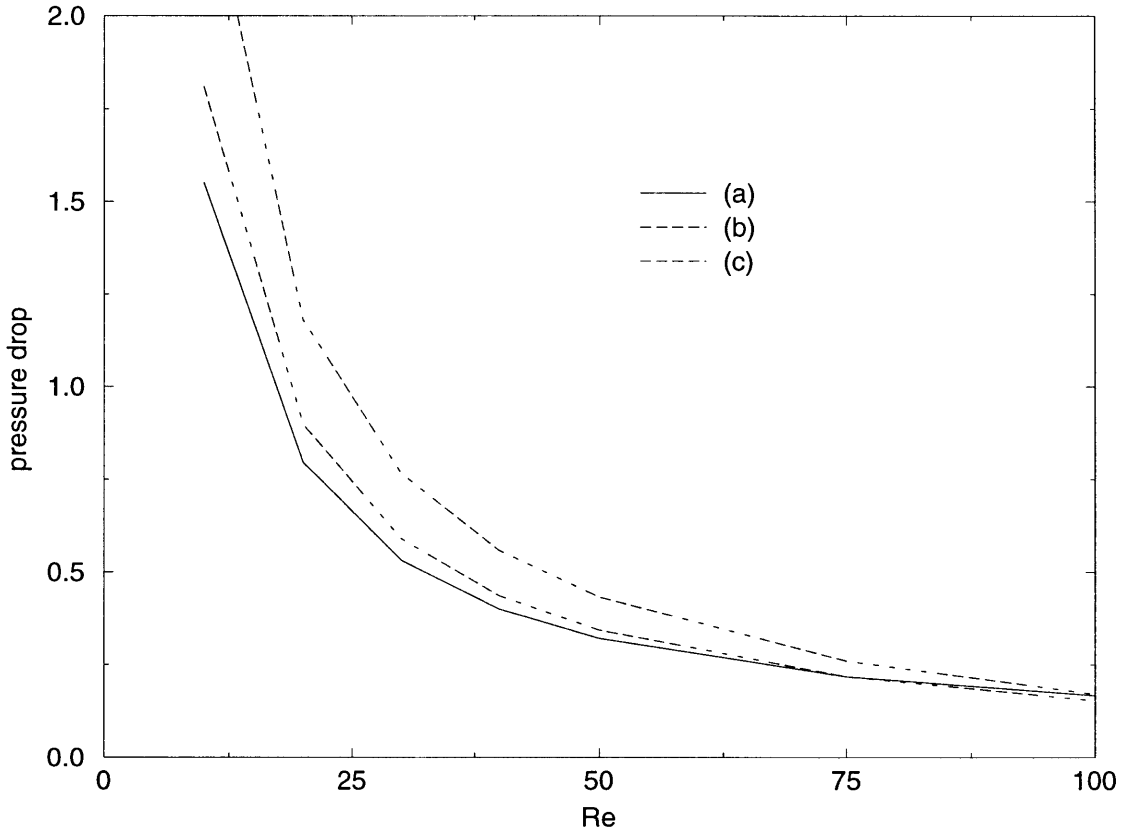

Fig. 4. Pressure drop in two-dimensional flow vs. *Re* for $\gamma = 0$, $\lambda_x = 1.0$ and (a) $\beta = 0.0$, (b) $\beta = 0.1$ and (c) $\beta = 0.175$.

parameters $Re = 156$, $\beta_x = 0.125$, $\beta_z = 0.0755$, $\lambda_x = 10/3$, $\alpha = 17.2^\circ$. For a two-dimensional geometry in which $\beta_x = 0.15$, and $\beta_z = 0$, the other parameters being the same, the value is 0 ± 0.25. This is further evidence that the particle paths can be chaotic in the eggcarton geometry.

6.2. Heat transfer

The isotherms shown in Fig. 10 for a eggcarton geometry are seen to be affected by the presence of the recirculating flow. The corresponding Nusselt number distribution is shown in Fig. 11. As the Peclet number increases, the peak-to-peak variation and asymmetry of *Nu* about the channel center, $x = 0$, becomes more pronounced in the eggcarton geometry, as was also the case in the corresponding two-dimensional corrugations.

It is interesting to analyze the variation of the Nusselt number with the flow angle α as shown in Fig. 12. For flows with a very slight z-component, there is an increase in $\langle Nu \rangle / \langle Nu_0 \rangle$. As α increases further, there is a sudden drop in the heat transfer, then a gradual rise. In order to understand this behavior, we must consider pathlines in the eggcarton channel. As described before, heat transfer enhancement in two-dimensional corrugations is due to the presence of stagnation points and an asymmetry of the flow. It is limited, however, by conduction across the bounding streamline which connects the two stagnation points. For the eggcarton geometry with $\alpha = 0$, the hydrodynamics are essentially the same. But, as seen in Fig. 9, even a small non-zero α results in pathlines which cross between the recirculation region and the main flow, producing an increase in convective heat transfer. As long as the overall flow structure does not vary significantly from that for a two-dimensional corrugated channel, the primary enhancement mechanism will still be due to the recirculating flow, but with an additional enhancement due to advective transport across the boundary of the recirculation region. However, as the transverse flow becomes stronger, the residence time of particles within the recirculation region becomes shorter and the region itself is destroyed; the heat transfer rate falls. For $\alpha > 8^\circ$, the ratio $\langle Nu \rangle / \langle Nu_0 \rangle$ increases again indicating that the amount of mixing within the main flow does provide

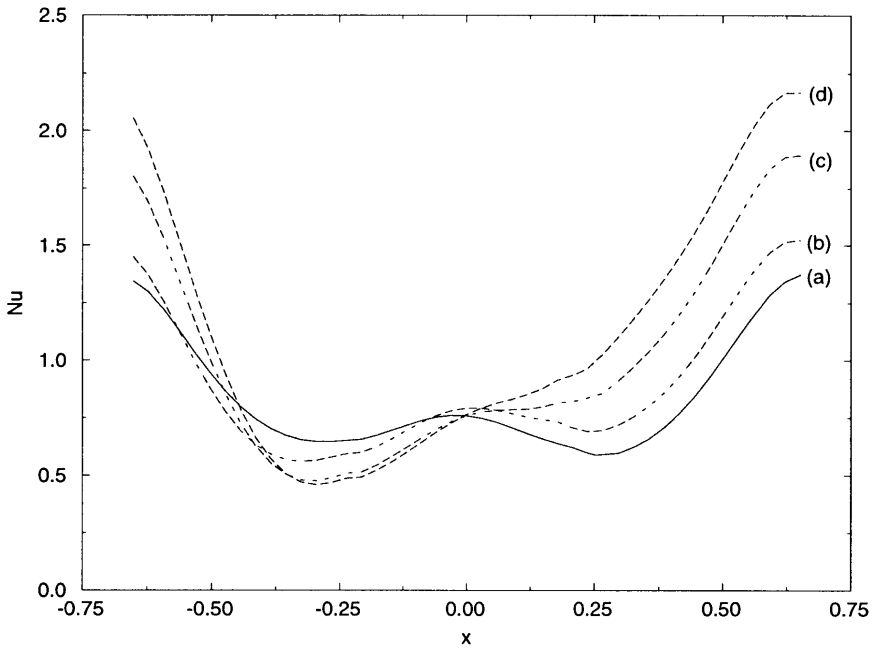

Fig. 5. Two-dimensional corrugations: local Nusselt number distribution from numerical solution; $Re = 100$, $\beta_x = 0.15$, $\lambda_x = 4/3$ and (a) $Pe = 0.01$, (b) $Pe = 10$, (c) $Pe = 50$, (d) $Pe = 100$.

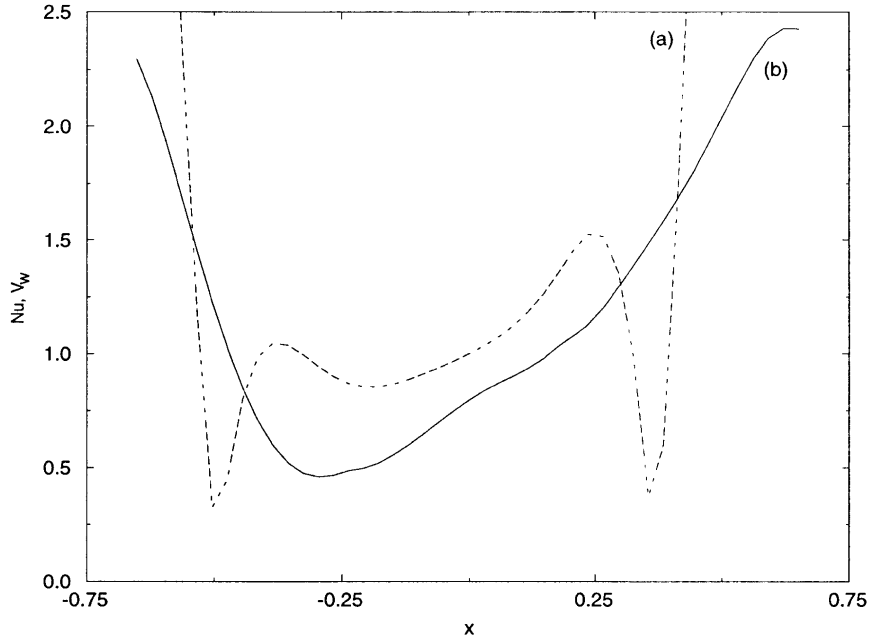

Fig. 6. Two-dimensional corrugations: (a) magnitude of the near-wall velocity (normalized by its value at $x = 0$) and (b) average Nusselt number from numerical solution; $Re = 100$, $\beta_z = 0.15$, $\lambda_x = 4/3$, and $Pe = 100$.

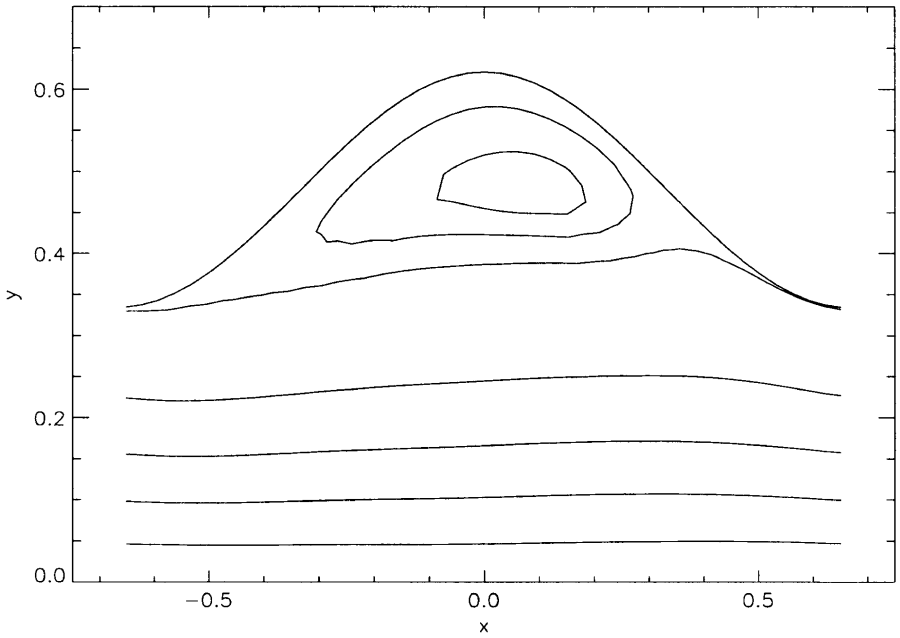

Fig. 7. Two-dimensional corrugations: streamlines from numerical solution; $Re = 100$, $\beta_x = 0.15$, $\lambda_x = 4/3$. Main flow from left to right.

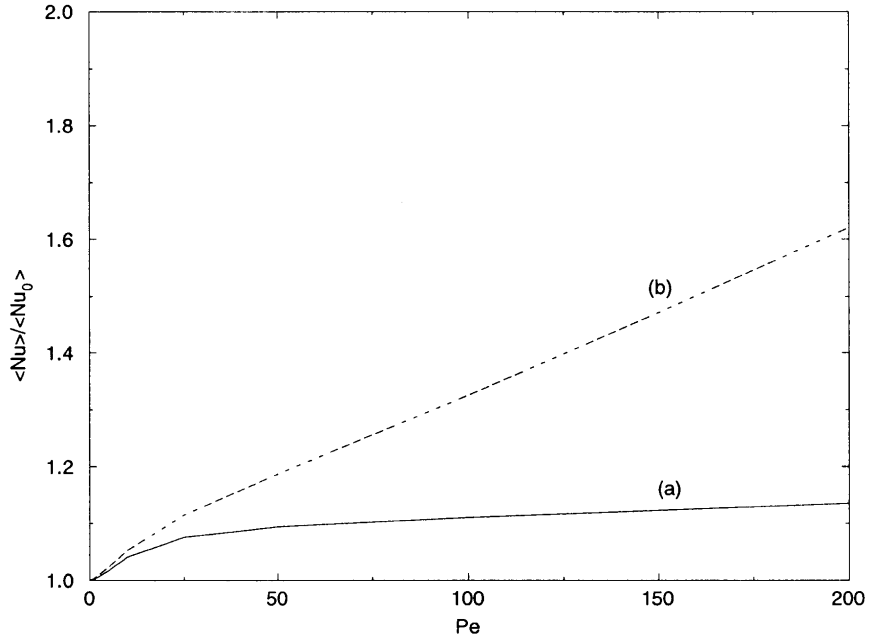

Fig. 8. Two-dimensional corrugations: heat transfer enhancement from numerical solution in (a) artificial, symmetric flow and (b) correct, asymmetric flow; $Re = 100$, $\beta_x = 0.15$, $\lambda_x = 4/3$.

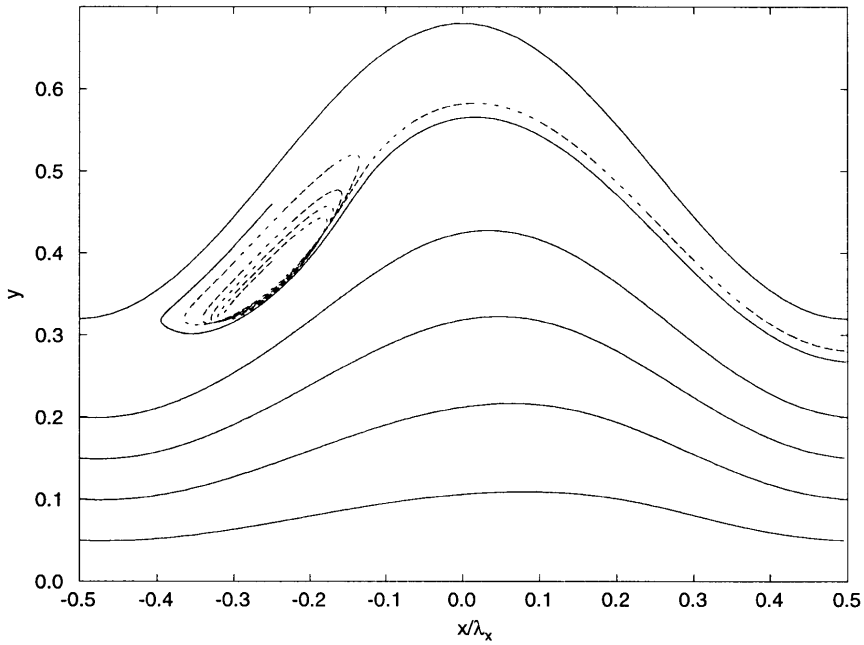

Fig. 9. Eggcarton corrugations: x–y projection of pathlines from perturbation solution; $Re = 350$, $\beta_x = 0.18$, $\beta_x = 0.02$, $\lambda_x = 10$, $\lambda_z = 100$, $\alpha = 5.7^\circ$. Main flow from left to right.

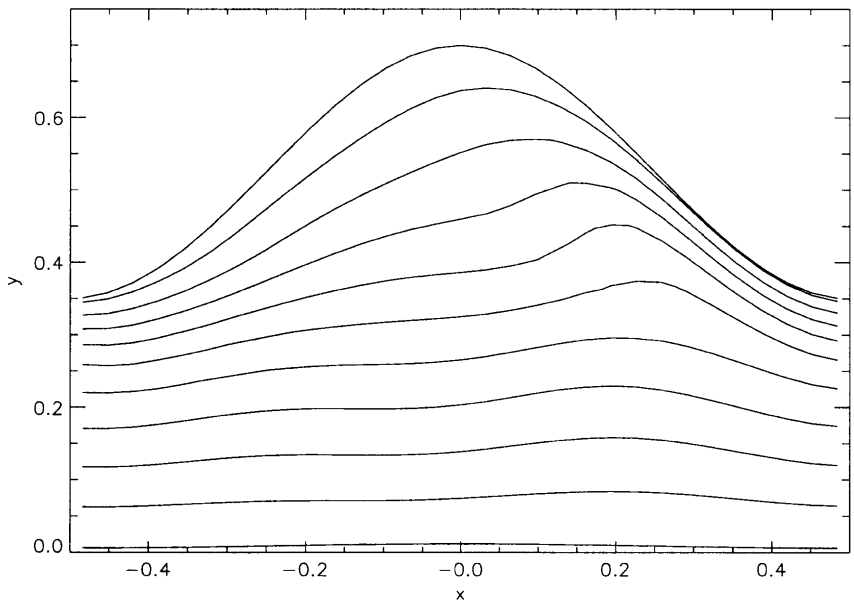

Fig. 10. Eggcarton corrugations: isotherms at $z = 0$; $Re = 141$, $\beta_x = 0.175$, $\beta_z = 0.025$, $\lambda_x = \lambda_z = 1$, $\alpha = 45^\circ$ and $Pe = 100$.

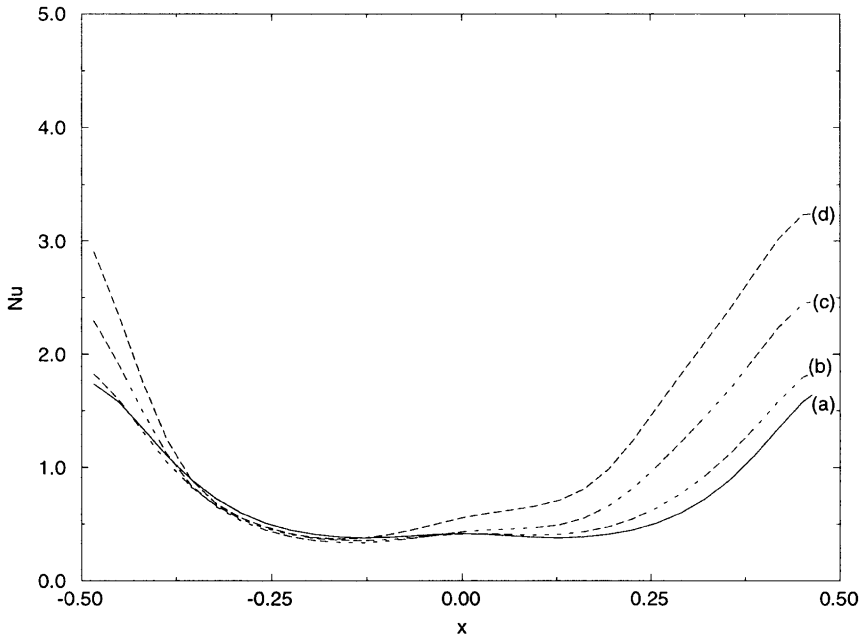

Fig. 11. Eggcarton corrugations: local Nusselt number distribution at $z = 0$; $Re = 141$, $\beta_x = 0.174$, $\beta_z = 0.025$, $\lambda_x = \lambda_z = 1$, $\alpha = 45^\circ$ and (a) $Pe = 0.01$, (b) $Pe = 10$, (c) $Pe = 50$, (d) $Pe = 100$.

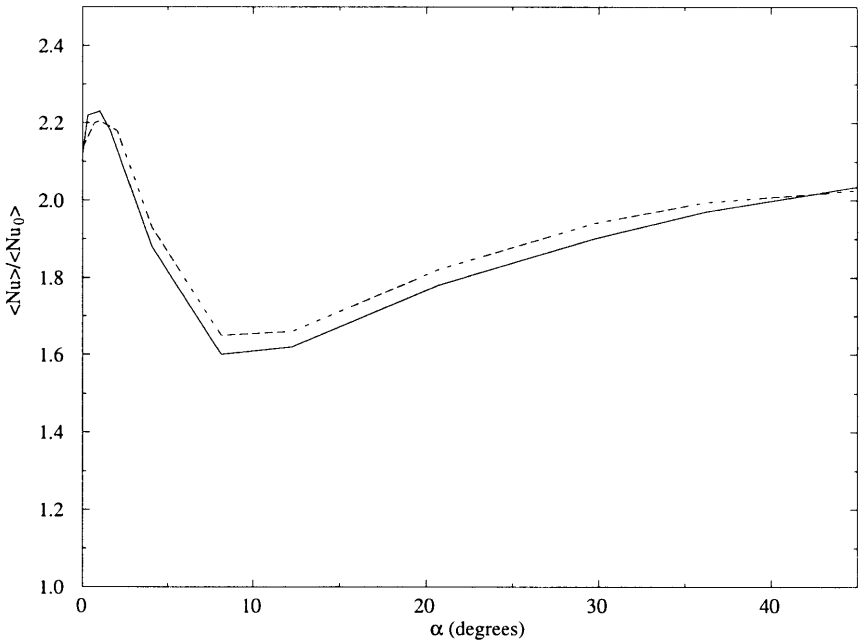

Fig. 12. Eggcarton corrugations: effect of flow alignment on heat transfer enhancement; $\beta_x = \beta_z = 0.1$, $\lambda_x = \lambda_z = 1$, $Pe = 200$ and (a) $Re = 141$, and (b) $Re = 212$.

some enhancement, but does not quite make up for the loss of the recirculation region.

There are several different ways in which the performance of this geometry can be quantitatively compared to that of the two-dimensional. For example, we can have the total amplitude $\beta_x+\beta_z$ the same, as shown in Fig. 13. When advection is important, i.e. for large Peclet numbers, the two-dimensional geometry does better; the enhancement is 14.8% at $Pe = 200$. Or we can compare the two geometries with the same surface area, as in Fig. 14. Now the eggcarton is better, the improvement being 17.4% at $Pe = 200$; the performance of both become similar as we go to the other extreme of pure conduction and $Pe \to 0$.

7. Conclusion

Local heat transfer enhancement in a channel with two-dimensional corrugations compared to flat plates is due to the presence of recirculation. At the upstream stagnation point fluid is pushed away from the heated upper wall; near the downstream stagnation point cool fluid is pushed toward the wall. As a result, the isotherms are distorted, creating a lower heat flux along the wall near the upstream stagnation point, and a higher heat flux near the downstream stagnation point. Area-average heat transfer enhancement is due primarily to the asymmetry of the recirculating flow with respect to the location of the stagnation points. If this asymmetry is removed artificially, the area-averaged Nusselt number decreases significantly. Since the actual flow is skewed toward the downstream stagnation point, the heat transfer enhancement in this region outweighs the inhibiting effect of the flow near the upstream stagnation point. The convective heat transfer depends on both temperature gradient and velocity, and the velocity normal to the wall is higher near the downstream stagnation point than that near the upstream stagnation point.

For slight three-dimensionality in the flow in a channel with eggcarton geometry the bounding surface between recirculating region and main flow becomes permeable. Although the recirculation region is still present for weak transverse flow rates, the fluid is able to move between this region and the mid-channel flow. This allows heat transfer across what was a barrier to advection in the two-dimensional corrugated channel. The result is an increase in the Nusselt number. As the flow angle α is increased further, the residence time of particles within the recirculation region is reduced. This has the ultimate effect of destroying the recirculation which is the primary source of heat transfer enhancement in both corrugated and eggcarton channels.

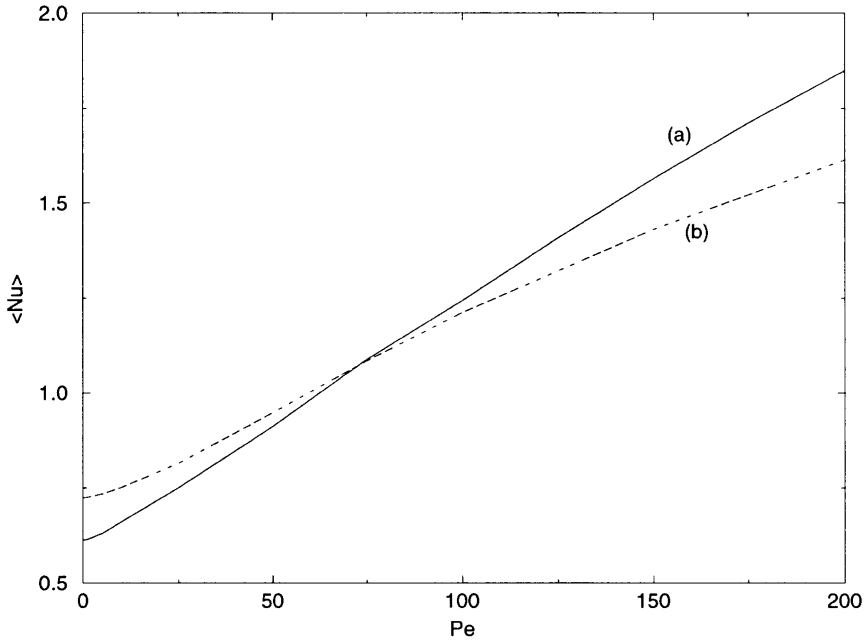

Fig. 13. Comparison of thermal performances with $Re = 100$ and same total amplitude of corrugations of (a) two-dimensional corrugations with $\beta_x = 0.2$, $\lambda_x = 1$ and (b) eggcarton geometry with $\beta_x = 0.1$, $\beta_z = 0.1$, $\lambda_x = 1$, $\lambda_z = 1$, $\alpha = 45^\circ$.

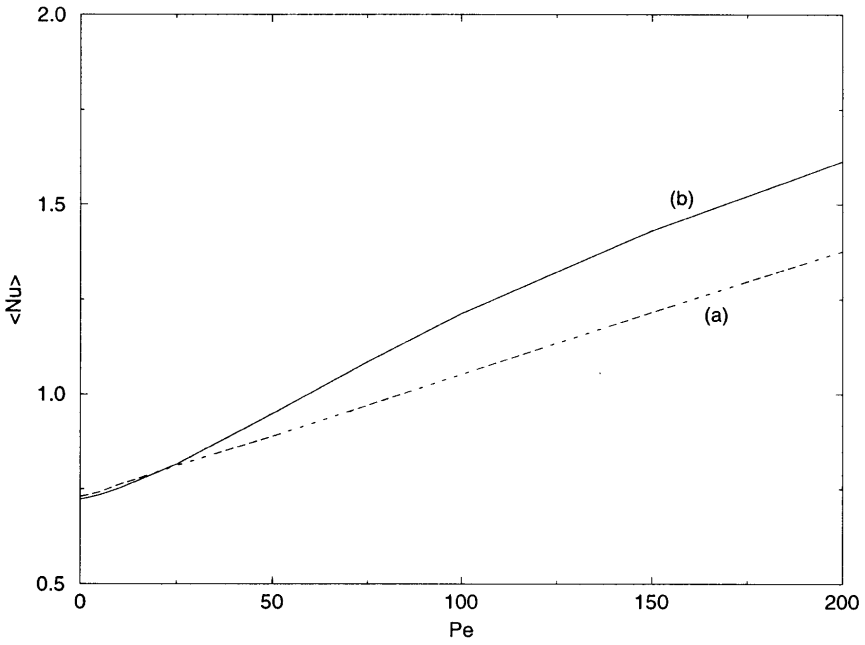

Fig. 14. Comparison of thermal performances with $Re = 100$ and same surface area of (a) two-dimensional corrugations with $\beta_z = 0.143$, $\lambda_x = 1$ and (b) eggcarton geometry with $\beta_z = 0.1$, $\beta_z = 0.1$, $\lambda_x = 1$, $\lambda_z = 1$, $\alpha = 45^\circ$.

Acknowledgment

We thank Dr M. C. Sharatchandra for help with the numerical method.

References

[1] Chow JCF, Soda K. Laminar flow and blood oxygenation in channels with boundary irregularities. J Appl Mech 1973;40:843–9.
[2] Sobey IJ. On flow through furrowed channels, Part 1, calculated flow patterns. J Fluid Mech 1980;96:1–26.
[3] Amano RS. A numerical study of laminar and turbulent heat transfer in a periodically corrugated wall channel. J Heat Transfer 1985;107:564–9.
[4] Sunden B, Trollheden S. Periodic laminar flow and heat transfer in a corrugated two-dimensional channel. Int Comm Heat Mass Transfer 1989;16:215–25.
[5] Goldstein L, Sparrow EM. Heat/mass transfer characteristics for flow in a corrugated wall channel. J Heat Transfer 1977;99:187–95.
[6] Asako Y, Faghri M. Finite-volume solutions for laminar flow and heat transfer in a corrugated duct. J Heat Transfer 1987;109:627–34.
[7] Molki M, Yuen CM. Effect of interwall spacing on heat transfer and pressure drop in a corrugated-wall duct. Int J Heat Mass Transfer 1986;29:987–97.
[8] Xin RC, Tao WQ. Numerical predictions of laminar flows and heat transfer in wavy channels of uniform cross-sectional areas. Num Heat Transfer 1988;14:465–81.
[9] Ali MM, Ramadhyani S. Experiments on convective heat transfer in corrugated channels. Experimental Heat Transfer 1992;5:175–93.
[10] Nishimura T, Ohiri Y, Kajimoto Y, Kawamura Y. Mass transfer characteristics in a channel with symmetric wavy wall for steady flow. J Chem Engng Japan 1985;18:550–5.
[11] Ghosh S, Chang H-C, Sen M. Heat transfer enhancement due to slender recirculation and chaotic transport between counter-rotating eccentric cylinders. J Fluid Mech 1992;238:119–54.
[12] Acharya N, Sen M, Chang H-C. Heat transfer enhancement in coiled tubes by chaotic mixing. Int J Heat Mass Transfer 1992;35:2475–89.
[13] Chang H-C, Sen M. Application of chaotic advection to heat transfer. Chaos, Solitons and Fractals 1994;4:955–75.
[14] Stasiek J, Collins MW, Ciofalo M, Chew P. Investigation of flow and heat transfer in corrugated passages—I. Experimental results. Int J Heat Mass Transfer 1996;39:149–64.
[15] Ciofalo M, Stasiek J, Collins MW. Investigation of flow and heat transfer in corrugated passages—II. Numerical simulations. Int J Heat Mass Transfer 1996;39:165–92.
[16] Gaiser G, Kottke V. Flow phenomena and local heat and mass transfer in corrugated passages. Chem Eng Tech 1989;12:400–5.
[17] Focke WW, Zachariades J, Oliver I. The effect of the corrugation inclination angle on the thermohydraulic performance of plate heat exchangers. Int J Heat Mass Transfer 1985;28:1469–79.
[18] Focke WW, Knibbe PG. Flow visualization in parallel-plate ducts with corrugated walls. J Fluid Mech 1986;165:73–7.
[19] Sawyers DR. Heat transfer enhancement by regular and

chaotic mixing in laminar channel flow. Ph.D. dissertation, Department of Aerospace and Mechanical Engineering, Notre Dame, IN 46556 : University of Notre Dame, 1997.
[20] Eringen AC. Nonlinear theory of continuous media. McGraw-Hill, 1962.
[21] Patankar SV. A calculation procedure for two-dimensional elliptic situations. Num Heat Trans 1981;4:409–25.
[22] Sharatchandra MC, Rhode DL. New, strongly conservative finite-volume formulation for fluid flows in irregular geometries using contravariant velocity components: Part 1, Theory. Num Heat Trans B 1994;26:39–52.
[23] Wolf A, Swift JB, Swinney HL, Vastano JA. Determining Lyapunov exponents from a time series. Physica D 1985;16:285–317.